Advances in Science and Technology Research Journal

Advances in Science and Technology Research Journal, 2026, 20(3), 409–423
https://doi.org/10.12913/22998624/213787
ISSN 2299-8624, License CC-BY 4.0

Received: 2025.10.14
Accepted: 2025.12.16
Published: 2026.02.01

Numerical analysis of rotation step and tracking strategy in flat-plate solar collectors: Thermal performance and cost-effectiveness

Robert Kowalik[1*], Aleksandar Nešović[2]

[1] Faculty of Environmental Engineering, Geodesy and Renewable Energy, Kielce University of Technology, Tysiaclecia P.P. 7, 25-314 Kielce, Poland
[2] Institute for Information Technologies, University of Kragujevac, Jovana Cvijića bb, 34000 Kragujevac, Republic of Serbia
* Corresponding author's e-mail: rkowalik@tu.kielce.pl

ABSTRACT

This study presents a numerical analysis of Sun-tracking strategies for flat-plate solar collectors, with emphasis on the influence of discrete rotation step size and control strategy on thermal performance. Two distinct control approaches were examined: absolute Sun tracking (aSAT), which continuously aligns the collector with the solar position, and relative Sun tracking (rSAT), which performs incremental angular adjustments. A total of sixteen configurations were simulated, combining both tracking strategies with eight discrete rotation step angles $\psi = \{1°, 2°, 5°, 10°, 15°, 30°, 45°, 90°\}$. Simulations were conducted using EnergyPlus 9.6 coupled with a custom Python interface, allowing one-minute resolution control of collector orientation. This framework enabled a detailed assessment of the effect of actuator precision on incident solar radiation and useful thermal gain. A temperature-dependent efficiency model, based on the Hottel–Whillier formulation, was implemented to account for heat losses as a function of ambient temperature and irradiance. Results demonstrate that increasing the rotation step ψ leads to a nonlinear decrease in collected energy, with energy losses reaching approximately 9% when ψ increases from 1° to 90°. The optimal balance between performance and mechanical simplicity was found for $\psi = 10–15°$, where the system retained over 90% of the energy yield of a continuously tracking collector. Absolute tracking (aSAT) achieved up to 17% higher daily energy gain compared to relative tracking (rSAT), especially for fine rotation steps. Although economic aspects were not included, the results provide clear design guidance for optimizing Sun-tracking mechanisms in flat-plate solar thermal systems. The developed numerical framework may support further experimental validation and the integration of tracking algorithms in low-energy and near-zero-energy buildings (nZEBs) under varying climatic conditions.

Keywords: single-axis tracking, flat-plate solar collector, rotation step, control strategy, solar radiation, EnergyPlus, relative vs. absolute tracking.

INTRODUCTION

The decarbonization of the building sector is a key priority in achieving global climate and energy targets. According to the International Energy Agency (IEA), solar thermal technologies are expected to contribute significantly to reducing fossil fuel dependency in space and water heating, potentially covering over 20% of low-temperature heating demand by 2050. In this context, improving the performance, adaptability, and control of flat-plate solar collectors (FPSC) remains a vital component of the global energy transition. FPSC systems are widely adopted due to their structural simplicity, low cost, and suitability for various climatic zones. These collectors are primarily used in domestic hot water production, space heating, and solar-assisted thermal systems. Solar energy technologies are generally categorized into three major groups: solar thermal

collectors, photovoltaic (PV) modules, and hybrid photovoltaic–thermal (PVT) systems that simultaneously convert solar radiation into heat and electricity [1–3]. Regardless of application, all such systems may operate in either a fixed (non-tracking) configuration or incorporate active sun-tracking mechanisms [4,5].

Tracking systems are further classified by their control strategy (open-loop, closed-loop, hybrid), drive type (active or passive), degrees of freedom (single-axis tracking – SAT, dual-axis tracking – DAT), and the tracking method (sensor-based, time-based, or combined) [6–12]. A schematic comparison of SAT and DAT mechanisms is presented in Figure 1, highlighting the mechanical and operational differences between both approaches.

Single-axis tracking (SAT) systems enable solar collectors to rotate about a single predefined axis, typically to maintain an orientation as close as possible to normal incidence with respect to incoming solar radiation. Among various configurations, alignment along the north–south meridian is generally considered the most effective [13]. Based on optimized angular positioning, [14] proposed a discrete SAT design that activates only three times per day. Despite its simplicity, experimental results demonstrated that this approach can achieve approximately 90–94% of the energy yield of a fully continuous tracking system. SAT configurations vary and may include vertical, horizontal, tilted horizontal, or polar-aligned axes. Compared to DAT systems, SATs offer notable advantages in terms of lower cost and mechanical simplicity, albeit at the expense of reduced tracking accuracy and energy capture [15–17].

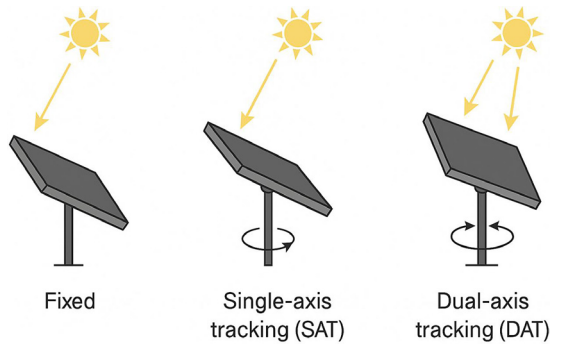

Figure 1. Diagram comparing SAT and DAT

A comparative summary of their efficiency potential, technical complexity, and typical implementation contexts is shown in Table 1.

Numerous studies confirm that sun-tracking can significantly enhance solar energy collection. Average energy gains range from 30–35% for SAT to 40–45% for DAT systems relative to fixed configurations [24]. However, most of these studies focus on idealized or fully dynamic tracking, often under highly favorable climate conditions such as Mediterranean, desert, or subtropical zones. Unlike such settings, this study addresses a Central European location (Kragujevac, Serbia), where seasonal variability, solar elevation, and cloud cover introduce additional design and control challenges for tracking systems.

Neville [25] developed two distinct mathematical models to evaluate the thermal performance of flat-plate solar collectors (FPSCs): one for systems equipped with single-axis tracking (SAT), and another for dual-axis tracking (DAT). Subsequent theoretical investigations [26] confirmed the viability of the DAT concept, indicating potential improvements in thermal efficiency exceeding 20% compared to non-tracking systems. Thomson [27,28] conducted both theoretical and experimental analyses comparing fixed-position FPSCs and DAT-equipped units under the climatic conditions of Tallinn, Estonia. The findings demonstrated a seasonal energy gain of approximately 10–20% in favor of the tracking systems.

Thermal performance metrics vary depending on the orientation and type of tracking mechanism. As reported in [29], FPSCs can achieve the following thermal efficiencies: 57.12% for N–S tracking around an E–W horizontal axis, 62.17% for E–W tracking around an N–S horizontal axis, 59.51% for E–W tracking around a vertical axis,

Table 1. Comparison of performance and design complexity of solar tracking systems in flat-plate collectors (based on data from [15–23])

System type	Number of axes	Efficiency gain compared to fixed system [%]	Technical complexity	Typical application
Fixed	0	0%	Very low	Small-scale, low-cost domestic installations
SAT	1	30–35%	Moderate	Residential buildings, nZEB
DAT	2	40–45%	High	Large-scale or specialized solar systems

64.36% for E–W tracking around an inclined N–S axis, and up to 67.25% for dual-axis tracking.

Various approaches to modeling the thermal behavior of fixed and tracking collectors have been proposed in the literature [30–32], encompassing both analytical and numerical frameworks. A comprehensive review, which also addressed the economic feasibility of tracking FPSCs, was presented in [33]. Furthermore, the impact of diffuse solar radiation—modeled using isotropic and anisotropic formulations accounting for ground reflectance and cloud cover—has been explored for both fixed and dual-axis tracking configurations [34].

Neagoe et al. [35] developed and experimentally validated an adaptive tracking algorithm for flat-plate solar collectors (FPSCs), introducing inverse tracking as an effective strategy to prevent overheating. Under the climatic conditions of Shtip (North Macedonia), Chekerovska and Filkoski [36] investigated the impact of solar tracking on FPSC efficiency through experimental testing supported by a validated 3D mathematical model. Ajunwa et al. [37] performed a TRNSYS-based simulation study on an FPSC system designed for solar drying, equipped with manually adjustable east–west side reflectors and a SAT mechanism. Optimal reflector angles were identified as 80°/45° for January and 80°/40° for February and March. Implementation of the SAT mechanism led to a 5.11% increase in total moisture reduction.

Furthermore, current literature lacks a systematic assessment of how discrete rotation step sizes (e.g., 5°, 15°, 30°) affect tracking efficiency in FPSC systems. These steps are dictated by actuator constraints in real-world installations and can significantly impact incident radiation and control precision. Additionally, a clear distinction between absolute and relative sun-tracking strategies defined in this study as aSAT and rSAT, respectively is largely absent in previous work. This conceptual differentiation is introduced here as a novel framework for understanding and optimizing control algorithms in simplified or cost-constrained solar tracking systems.

From a methodological perspective, this research offers a new approach by leveraging EnergyPlus a widely used building energy simulation engine—to simulate high-resolution solar tracking. A custom Python interface enables minute-by-minute time resolution, allowing for accurate simulation of stepwise orientation adjustments and their influence on collector irradiance. This time-resolved framework provides new insight into the interplay between tracking step, strategy, and site-specific solar availability.

This study analyzes a flat-plate solar collector with a single-axis tracking mechanism oriented east–west (E–W), rotating around a tilted north–south (N–S) axis. Eight discrete tracking step sizes (ψ = 1°, 2°, 5°, 10°, 15°, 30°, 45°, 90°) are evaluated under two control strategies: absolute tracking (aSAT) and relative tracking (rSAT). The simulations are performed for a clear-sky day (26 July) using real meteorological data from Kragujevac, Serbia.

Unlike previous works such as [24], which investigated photovoltaic trackers under idealized continuous motion, this study introduces discrete-step tracking and compares absolute and relative strategies for thermal collectors under Central European conditions.

Beyond its relevance to solar thermal researchers, the findings of this study may inform designers, simulation specialists, and automation engineers working on the integration of solar tracking systems in residential and near-zero energy buildings (nZEBs). The introduced framework offers practical guidance for balancing energy performance with mechanical simplicity and control logic, particularly in solar retrofitting, solar-assisted HVAC, and cost-optimized thermal systems.

Furthermore, the proposed numerical framework can be further enhanced in future research by coupling the current geometric and radiative model with advanced analytical formulations for transient heat transfer [38,39]. In particular, differential methods such as the Adomian decomposition technique [40] and analytical treatments of moving-boundary thermal systems [41] could be employed to solve nonlinear energy equations in solar collectors. These approaches may provide deeper insight into the dynamic temperature field within the absorber plate and improve the accuracy of predictive models for time-dependent solar performance.

MATERIALS AND METHODS

Simulation environment

Numerical simulations were performed using EnergyPlus 9.6, a widely adopted tool for energy modeling of buildings and HVAC systems. Since standard EnergyPlus does not support detailed control of solar tracking mechanisms, a custom

interface was developed in Python, enabling dynamic control of the collector's orientation by modifying tilt and azimuth values at 1-minute intervals. This data was fed into the simulation using the Energy Management System (EMS), allowing for precise emulation of tracking movements throughout the day.

Location and climatic conditions

Simulations were carried out for the city of Kragujevac, Serbia (latitude: 44.01°N, longitude: 20.91°E), which features a temperate continental climate. A clear-sky day July 26 was selected to examine the performance under maximum solar input. Weather data were obtained from the EnergyPlus EPW file for the location, including hourly values for global, diffuse, and direct irradiance.

Tracking configuration and geometry

The analyzed unit is a flat-plate solar collector with an effective surface area of 0.40 m² (500 × 800 mm), mounted on a movable structure that enables single-axis solar tracking. The tracking axis was inclined in the north–south (N–S) direction, allowing the collector to follow the Sun's daily movement in the east–west (E–W) plane. The maximum rotation range of the collector was ±90°, measured relative to its neutral position (facing east at sunrise). The collector tilt angle with respect to the horizontal was set to 34°, corresponding to the optimal summer configuration for the given geographic latitude. The orientation of the collector surface during tracking was described using the rotation of its normal vector around the local vertical axis:

$$\vec{n}(t) = R_z\big(\psi(t)\big) \cdot \vec{n}_0 \qquad (1)$$

where: $\vec{n}_0$ – initial surface normal vector (facing east at sunrise), $R_z\big(\psi(t)\big)$ – rotation matrix around the local vertical axis (Z-axis), ψ(t) – discrete rotation step at time t. The resulting vector n(t) was used to compute the tilt and azimuth angles of the collector in real time, which were passed to EnergyPlus as input variables.

Control strategies: absolute vs relative

Two different control strategies were implemented:

- absolute sun tracking (aSAT) – the collector rotates to a predefined absolute position, measured from a fixed reference (e.g., true east). Each movement is independent and calculated from the base orientation.
- relative sun tracking (rSAT) – the collector adjusts its position relative to its current orientation, incrementing by a fixed angle ψ at each step. This approach better represents low-cost systems with time-based or manual control.

The distinction between aSAT and rSAT is critical in real-world applications, as it affects both energy performance and controller complexity.

Rotation step scenarios

To analyze the impact of tracking precision on collector performance, eight discrete rotation step sizes were considered:

$$\psi = \{1°,2°,5°,10°,15°,30°,45°,90°\} \qquad (2)$$

Each angle was applied under both control strategies (aSAT and rSAT), resulting in a total of 16 simulation scenarios. The tilt and azimuth values were computed for each case and converted into solar coordinates using local solar time and the geographic position of the collector. A full overview of the simulation scenarios is presented in Table 2. The ψ = 1° case approximates near-continuous tracking, providing a practical upper limit for actuator-based systems.

Assumptions and limitations

To isolate the impact of tracking resolution and control strategy on collector exposure, several simplifying assumptions were applied in the simulation model: The solar collector was represented as an idealized surface with perfect optical absorption. Thermal losses, conversion efficiency, and heat transfer mechanisms were not modeled. Mechanical tracking was assumed to operate with no time delay or energy loss. Inertia, backlash, and actuator constraints were neglected. Environmental influences such as shading, surface soiling, reflection from nearby objects, and wind were not considered. The analysis focused exclusively on calculating the total solar radiation incident on the collector surface throughout the day. These assumptions allowed for a controlled numerical comparison across scenarios while minimizing the influence of secondary factors unrelated to tracking geometry

Table 2. Simulation scenarios for different rotation steps and strategies

Scenario ID	Tracking strategy	Rotation step ψ [°]	Scenario number
aSAT_1deg	aSAT	1	1
aSAT_2deg	aSAT	2	2
aSAT_5deg	aSAT	5	3
aSAT_10deg	aSAT	10	4
aSAT_15deg	aSAT	15	5
aSAT_30deg	aSAT	30	6
aSAT_45deg	aSAT	45	7
aSAT_90deg	aSAT	90	8
rSAT_1deg	rSAT	1	9
rSAT_2deg	rSAT	2	10
rSAT_5deg	rSAT	5	11
rSAT_10deg	rSAT	10	12
rSAT_15deg	rSAT	15	13
rSAT_30deg	rSAT	30	14
rSAT_45deg	rSAT	45	15
rSAT_90deg	rSAT	90	16

or control. A constant mean temperature of 50 °C was assumed to represent typical domestic hot water operation and to isolate tracking effects from transient thermal behavior. The selected absorber area (0.40 m²) serves as a normalized reference, as results scale linearly with surface area.

Meteorological data

Hourly profiles of total H_{tot} [W/m²], direct H_{beam} [W/m²], and diffuse H_{diff} [W/m²] terrestrial solar radiation received by a horizontal surface in Kragujevac (φ = 44.02°N, λ = 20.92°E) on July 26 are shown in Figure 2.

For July 26 (clear day, sunrise at 04:23 h, sunset at 19:03 h), the following average daily values were measured (Figure 4): $H_{tot,avg}$=667.61 W/m², $H_{beam,avg}$=525.83 W/m² and $H_{diff,avg}$=141.78 W/m². The maximum values were recorded at 13:30 h ($H_{tot,max}$=978 W/m²), 14:30 h ($H_{beam,max}$=838 W/m²) and 11:30 h ($H_{diff,max}$=258 W/m²). The cloudy-sky periods (which can be concluded from the discontinuity of the terrestrial beam solar radiation curve) are present in the period from 07:30 h to 15:00 h.

During the mentioned period for the analyzed location, the wind speed c_w [m/s] (Figure 5) is variable, but it is within the limits between $c_{w,min}$=0.4 m/s (07:00 h) and $c_{w,max}$=3.1 m/s (17:00 h). Average daily air temperature is $t_{o,avg}$=21.81 °C (Figure 3). Minimum and maximum daily values are $t_{o,min}$=19.1 °C (04:00 h) and $t_{o,max}$=24.7 °C (15:00 h), respectively.

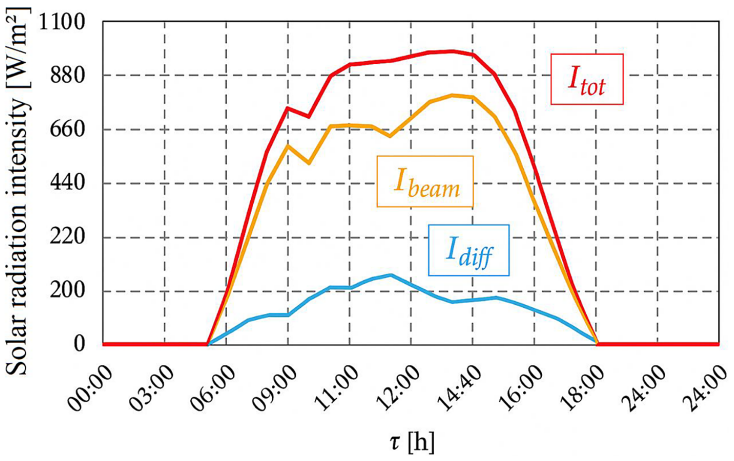

Figure 2. Terrestrial solar radiation on a horizontal surface during July 26 [42]

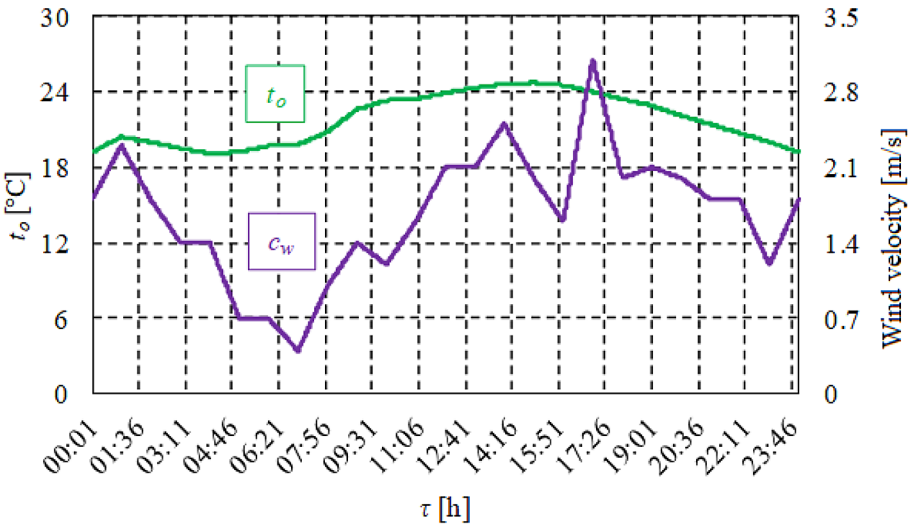

Figure 3. Air temperature and wind speed during July 26 [42]

SCENARIO SIMULATIONS

Since there are no models for analyzing tracking solar systems in the Energy Plus software, the models were artificially created for the purposes of this study.

Namely, through a series of simulations, the total incident solar radiation was calculated during the day, for each FPSC rotation angle in the E-W direction around the inclined N-S rotation axis: from -90° (the moment of sunrise) to +90° (the moment of sunset). The rotation angle was 1°. For the results to be as accurate as possible, the one-minute time step was used. The maximum numerical value for each rotation angle at a given time was used to form the daily curve of total incident solar radiation. In this way, a large database was created, which was then used to create different tracking scenarios, in this particular case, based on 8 rotation steps ψ [°]: ψ=1°, ψ=2°, ψ=5°, ψ=10°, ψ=15°, ψ=30°, ψ=45° and ψ=90°. All analyzed cases are graphically presented in Figure 4. Total incident solar radiation I_{tot} [W] on the tracking surface, i.e. FPSC with SAT, is determined by Equation 3:

$$I_{tot} = I_{beam} + I_{diff} + I_{refl} \qquad (3)$$

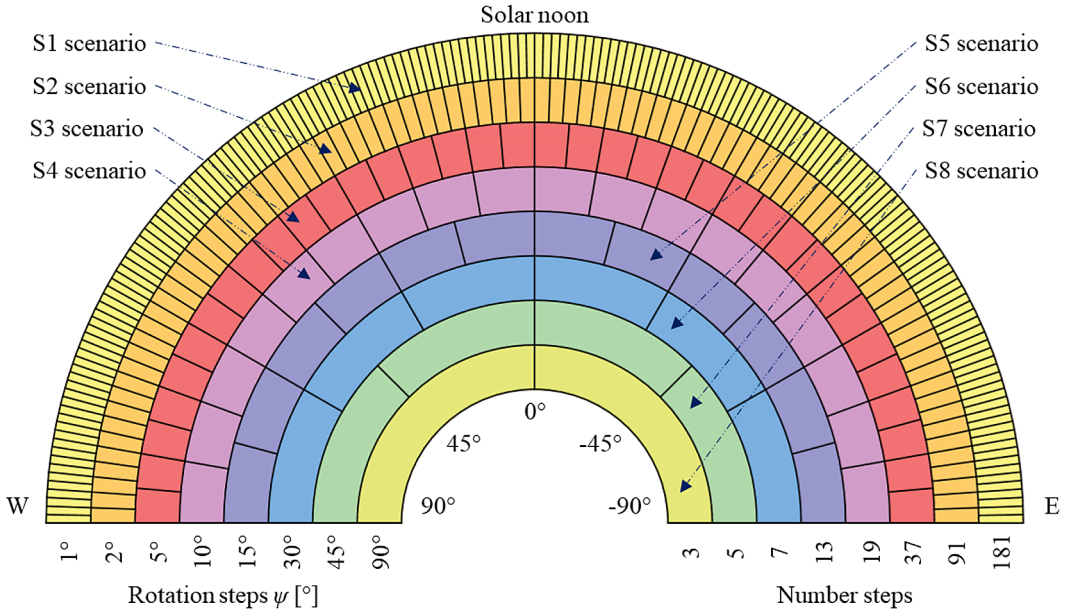

Figure 4. Tracking movement paths for selected scenarios (ψ = 1°, 15°, 90°) in aSAT and rSAT modes

where: [37]: I_{beam} [W] is the beam incident solar radiation, I_{diff} [W] is the diffuse incident solar radiation Equation 3 and I_{refl} [W] is the reflected incident solar radiation Equation 4.

$$I_{diff} = I_{diff,cr} + I_{diff,sd} + I_{diff,sh} \quad (4)$$

$$I_{refl} = I_{refl,beam} + I_{refl,diff} \quad (5)$$

where: [37]: $I_{diff,cr}$ [W] is the diffuse incident solar radiation from the circumsolar region, $I_{diff,sd}$ [W] is the diffuse incident solar radiation from the sky dome, $I_{diff,sh}$ [W] is the diffuse incident solar radiation from the sky horizon, $I_{refl,beam}$ [W] is the reflected beam incident solar radiation and $I_{refl,diff}$ [W] is the reflected diffuse incident solar radiation.

RESULTS AND DISCUSSION

The aim of this part of the study was to compare the effectiveness of two single-axis solar tracking strategies—absolute Sun tracking (aSAT) and relative Sun tracking (rSAT)—under varying rotation step angles (ψ). The numerical simulations were conducted for eight scenarios, where the collector was rotated in discrete angular increments of 1°, 2°, 5°, 10°, 15°, 30°, 45°, and 90°. Each scenario was evaluated for a clear summer day (July 26) under the climatic conditions of Kragujevac, Serbia (latitude 44.02°N, longitude 20.92°E).

Effect of rotation step angle in aSAT mode

In the aSAT strategy, the collector position is determined directly based on the real-time solar azimuth and elevation. This method ensures that the collector is oriented toward the Sun as precisely as the mechanical system allows. The simulations aimed to determine how reducing the angular resolution of the system i.e., increasing ψ affects the amount of solar radiation intercepted by the collector surface.

For each scenario, the hourly profile of incident solar radiation on the absorber surface was computed over the entire daylight period. These values serve as a proxy for potential thermal energy yield, as thermal performance is closely related to solar input under steady conditions. The results, visualized in Figure 5, clearly show the gradual decline in collected energy as the rotation step increases. This decline is particularly noticeable during early morning and late afternoon hours, where lower-resolution tracking (e.g., ψ = 45° or 90°) fails to align the collector adequately with the Sun's position. Notably, even relatively coarse adjustments (ψ = 10°–15°) still maintain a high level of efficiency compared to the finest resolution (ψ = 1°), suggesting that modest simplification of the control mechanism does not significantly compromise performance. However, beyond ψ = 30°, the performance drop becomes more pronounced, which may limit the usefulness of such configurations in applications

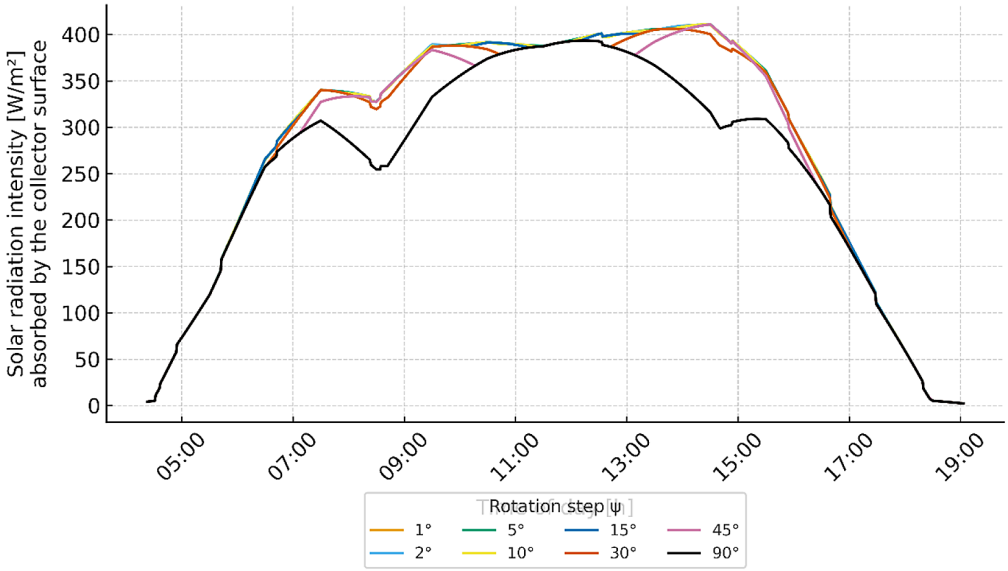

Figure 5. Daily profile of radiation intensity absorbed by a flat collector in aSAT mode for different rotation steps (ψ = 1°–90°)

where maximizing solar input is critical. As can be seen from the data presented, scenarios with high tracking precision (ψ = 1°–5°) provide almost identical and maximum radiation values throughout the day. The lines representing these cases are almost superimposed, suggesting that further reduction of the angle does not bring significant energy benefits.

As the rotation angle increases, the alignment of the collector with the Sun deteriorates, resulting in a gradual decrease in the intensity of absorbed radiation, especially in the morning and afternoon hours. The greatest losses are observed for the 90° step, where the collector changes position only twice during the day, resulting in a low and irregular yield profile. In this scenario, the energy obtained in the morning and evening hours drops to below 300 W/m², which is a significant limitation compared to solutions with smaller control angles.

The analysis of the graph therefore confirms that precise sun tracking is crucial for optimising the system's performance. Under simulation conditions, the minimum effective step is 5°, which can be considered a compromise between the complexity of the system and its efficiency.

Dependence of energy yield on rotation angle in aSAT mode

To better illustrate the impact of the rotation step angle (ψ) on the total daily energy gain under the aSAT strategy, a curve was fitted to the simulated data showing the relationship between ψ and solar energy received by the collector surface. A second-degree polynomial regression model was used to capture the trend, and the results are presented in Figure 6.

The analysis confirms a clear and consistent pattern: as the rotation step increases, the daily energy yield systematically decreases. The highest values are observed at the smallest rotation angles (1°–2°), which is in line with expectations—greater tracking precision allows the collector to remain more closely aligned with the actual solar position throughout the day.

The quadratic regression function fitted to the data demonstrated an excellent match, with a coefficient of determination $R^2 = 0.9992$. This high level of correlation suggests that the daily energy gain can be accurately predicted as a function of ψ. Such a precise mathematical relationship is particularly valuable in the early stages of system design, for example when selecting motor controllers or deciding on a trade-off between energy efficiency and mechanical simplicity (and cost).

It is also worth noting that for the largest simulated rotation step (ψ = 90°), the energy yield falls below 260 Wh/m², which corresponds to a loss of more than 9% compared to high-precision scenarios. This finding clearly demonstrates that in aSAT systems, minimizing the angular step can significantly improve overall energy performance, and should therefore be considered a priority in system optimization.

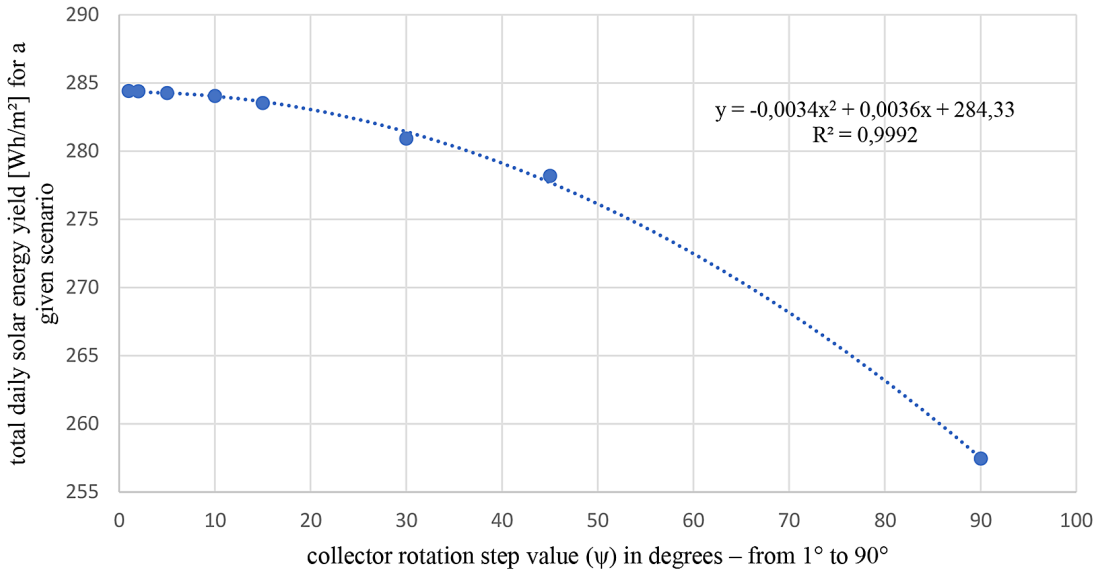

Figure 6. Effect of rotation angle ψ on daily solar energy yield in aSAT mode. The dotted line represents the fitted quadratic regression function ($R^2 = 0.9992$)

Effect of rotation step angle on radiation profile in rSAT mode

In a similar manner to the aSAT analysis, the daily radiation profile of a flat-plate collector operating under the relative rSAT strategy was examined. The analysis included eight different rotation step scenarios, ranging from $\psi = 1°$ to 90°, and the results are presented in Figure 7. For small rotation steps ($\psi \leq 5°$), the radiation curves remain nearly flat and consistently high throughout the day. This indicates good alignment between the collector surface and the direction of incoming solar rays, suggesting that, under fine-resolution control, rSAT can achieve energy performance comparable to that of the aSAT strategy.

However, starting from $\psi = 10°$, visible deviations begin to emerge, particularly during the morning and afternoon hours. These manifest as distinct "steps" or drops in the radiation profile, reflecting the system's inability to adequately track the Sun's movement with coarse angular adjustments. The effect is most pronounced for $\psi = 90°$, where the radiation curve becomes noticeably flattened and diverges from those of finer tracking scenarios. This behavior reveals the limited responsiveness of rSAT when operating at large step intervals, which inevitably leads to energy losses.

When compared to the radiation profiles observed under the aSAT strategy, it becomes evident that rSAT exhibits greater irregularity and less stability in energy gain. This is inherent to its control principle: the collector's current position depends solely on its previous state, rather than on the Sun's actual position. As a result, even minor delays or coarser adjustments can accumulate, degrading tracking accuracy over time.

Relationship between energy yield and rotation step angle in aSAT mode

For the aSAT strategy, a second-degree polynomial regression curve was constructed to describe the relationship between the collector's rotation step angle (ψ) and the total daily solar energy gain. The analysis included eight discrete scenarios, with ψ ranging from 1° to 90°. The resulting regression plot and the fitted function are presented in Figure 8.

As expected, the highest energy yields were observed for small rotation angles ($\psi = 1°–5°$), where the mechanical system is capable of frequently and accurately adjusting the collector's position to follow the real-time solar trajectory. In these cases, the daily energy yield reached up to 241.8 Wh/m².

With increasing rotation angle, the system's efficiency gradually declined. This reduction can be attributed to the growing angular mismatch between the incoming solar rays and the absorber surface normal. For the largest tested angle ($\psi = 90°$), the energy yield dropped below 225 Wh/m², representing an approximate 7% loss compared to the optimal configuration.

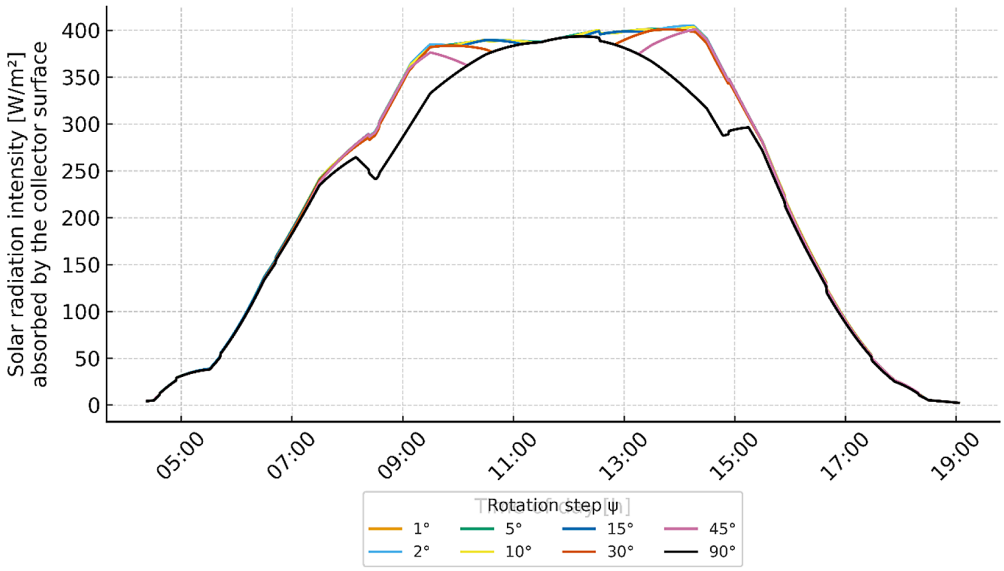

Figure 7. Daily profile of incident solar radiation absorbed by the flat-plate collector under rSAT mode for various rotation step angles ($\psi = 1°–90°$)

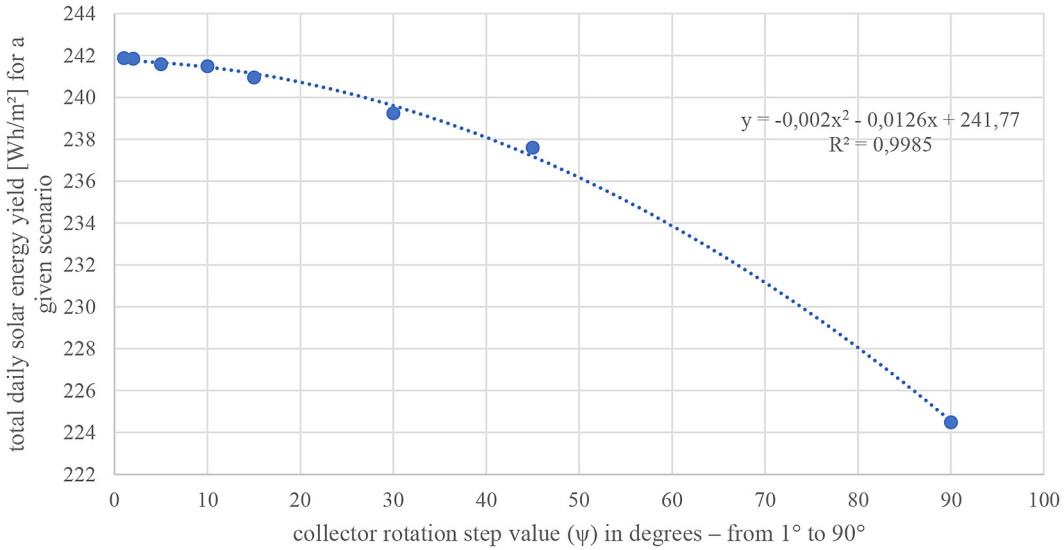

Figure 8. Influence of the rotation step angle ψ on daily solar energy gain under aSAT mode. The dashed line represents the fitted quadratic regression curve ($R^2 = 0.9985$)

The regression model's high coefficient of determination ($R^2 = 0.9985$) confirms excellent agreement with the simulation data. This strong correlation enables the use of the derived function in design and optimization processes, particularly in cases where it is necessary to balance mechanical complexity and energy performance. The model may be especially useful in the development of cost-efficient single-axis tracking systems for solar thermal applications in residential and low-energy buildings.

Comparison of tracking strategies: aSAT vs. rSAT

To directly compare the effectiveness of the two tracking strategies—absolute Sun tracking (aSAT) and relative Sun tracking (rSAT)—a combined analysis of daily energy yield as a function of rotation step angle (ψ) was conducted. The resulting graph is presented in Figure 9.

The results clearly show that aSAT consistently outperforms rSAT across the entire range of tested rotation angles. Since aSAT continuously

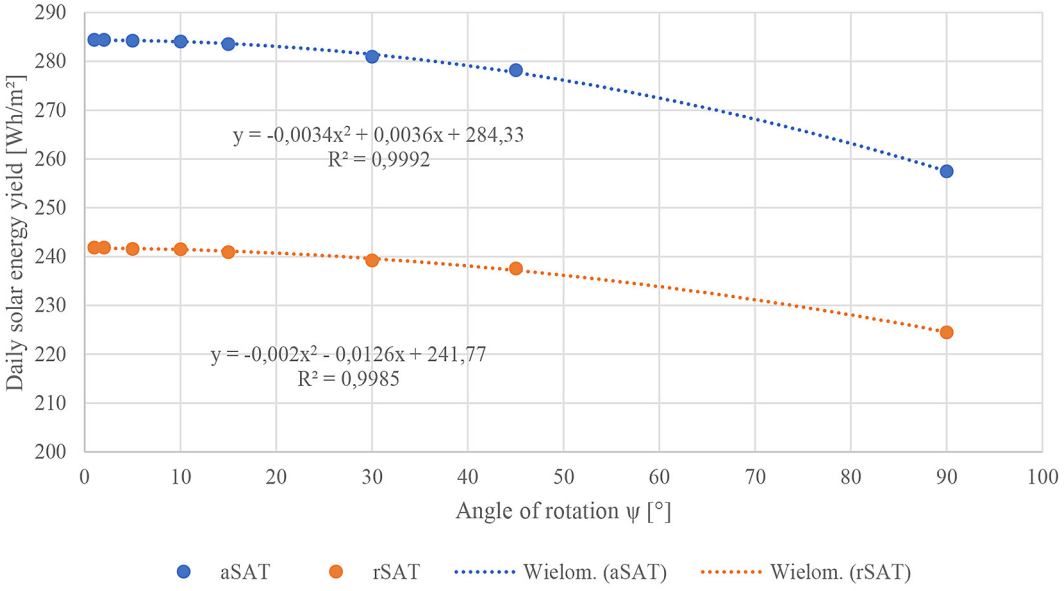

Figure 9. Comparison of daily energy yield [Wh/m²] as a function of rotation step angle ψ for aSAT and rSAT strategies. The dashed lines represent fitted quadratic regression curves

aligns the collector with the Sun's true position, it maintains a higher solar energy yield in every scenario. The difference is most pronounced at small rotation steps (ψ = 1°–5°), where aSAT provides up to 40–45 Wh/m² more energy than rSAT, corresponding to a 15–18% increase in efficiency.

As the rotation angle increases, both strategies experience a gradual decline in performance, which is expected due to the decreasing tracking precision. However, aSAT remains more effective even at the coarsest step (ψ = 90°). In this case, the energy advantage of aSAT over rSAT narrows to around 15 Wh/m², which still represents a meaningful difference over long operating periods, especially in year-round applications. For both strategies, the relationship between ψ and energy yield is well described by a second-degree polynomial regression, indicating that the efficiency loss with increasing step angle is nonlinear. This type of relationship is particularly valuable in practical system design, as it provides a visual and analytical basis for optimizing the balance between mechanical complexity and energy performance.

On average, the daily energy yield achieved by aSAT was 279.6 Wh/m², compared to 238.6 Wh/m² for rSAT. This means that absolute tracking generated approximately 41 Wh/m² more solar energy per day, which translates to a 17.1% overall advantage across the full range of ψ values. The largest differences were observed at ψ = 1°–5°, where aSAT held a performance edge of up to 17.6%, while at ψ = 90°, the difference narrowed to 14.6%. These results confirm that aSAT not only provides superior energy yield but also maintains better efficiency under simplified control conditions.

The obtained data may serve as a valuable design reference for selecting appropriate tracking strategies and control parameters in solar collector systems—particularly in building applications, where system cost, simplicity, and long-term performance must be carefully balanced.

Simplified thermal performance model

Although the numerical analysis conducted in this study focused exclusively on the geometric and radiative aspects of solar tracking, in practical solar thermal systems, the thermal efficiency of a flat-plate solar collector plays a crucial role in determining the net useful energy output. To estimate the potential thermal benefit of improved solar tracking precision, a simplified thermal performance model is introduced here.

Assumptions and model structure

To maintain analytical transparency while increasing physical realism, the collector is modeled as a quasi-steady system under clear-sky conditions. Rather than assuming a fixed thermal efficiency, the useful thermal energy gain Q_u is estimated using a temperature-dependent performance model based on the simplified Hottel–Whillier equation:

$$\eta(t) = \eta_0 - a_1 \cdot \frac{T_m(t) - T_a(t)}{I_{tot}(t)} \tag{6}$$

where: η_0 – 0.74 is the optical efficiency of the collector, a_1 –3.5 W/m²K is the overall heat loss coefficient, $T_m(t)$ is the average fluid/absorber temperature (assumed constant at 50 °C), $T_a(t)$ is the ambient air temperature (obtained from the simulation), $I_{tot}(t)$ is the total incident solar radiation on the collector surface.

A constant mean temperature of 50 °C was assumed to represent typical domestic hot water operation and to isolate tracking effects from transient thermal behavior.

$$Q_u(t) = \eta_{th} \cdot I_{tot}(t) \cdot A \tag{7}$$

where: η_{th} – thermal efficiency, $I_{tot}(t)$ – instantaneous incident radiation [W/m²], A – effective absorber area = 0.40 m².

The daily useful energy output, $Q_{u,day}$, is then estimated as:

$$Q_{u,day} = \eta_{th} \cdot \int_{t_{sunrise}}^{t_{sunset}} I_{tot}(t) \cdot A dt \tag{8}$$

This integral is evaluated numerically using the 1-minute resolution output from the EnergyPlus simulations. To maintain consistency with the simulation time resolution, the above equation is applied on a per-minute basis throughout the daylight period. The daily energy yield $Q_{u,day}$ is then computed as the numerical sum over the entire period. This model allows for more accurate estimation of thermal output compared to constant-efficiency assumptions, while still avoiding the complexity of full dynamic thermal simulations.

Results for 16 scenarios

Table 3 summarizes the estimated useful thermal energy gain for each of the 16 tracking scenarios (8 step sizes × 2 strategies). The results were initially calculated assuming a constant thermal efficiency of $\eta = 0.65$ to provide a simple comparative baseline. However, to improve physical accuracy, a temperature-dependent performance model was applied in Section 4.3, which adjusts efficiency dynamically based on ambient conditions. This dual approach enables comparison between simplified and more realistic thermal yield estimations, while maintaining consistency with previously published methodologies.

These results indicate that even under simplified thermal assumptions, the impact of the tracking strategy and rotation step is significant. The highest thermal gain (96.9 Wh/day) was achieved with aSAT and $\psi = 1°$, while the lowest (77.7 Wh/day) was observed for rSAT and $\psi = 90°$.

Temperature-dependent thermal model

To improve the realism of the thermal gain estimates, a temperature-dependent collector efficiency model was applied, based on the Hottel–Whillier Equation 6. The resulting effective collector efficiency was $\eta_{real} = 0.592$. Applying this to previously computed daily solar inputs, the adjusted thermal gains per day (Q_{real}) and annual thermal outputs were recalculated for selected cases. These are summarized in Table 4.

The numerical analysis clearly demonstrates that both the tracking strategy and the rotation step (ψ) have a substantial impact on the solar energy yield of flat-plate collectors. The absolute Sun tracking (aSAT) strategy—based on real-time alignment with the solar position—consistently produced the highest energy gains across all scenarios. Its advantage was particularly evident for small rotation steps ($\psi \leq 10°$), where aSAT outperformed the relative tracking (rSAT) approach by approximately 15–17% in daily solar input. In contrast, the rSAT strategy, which adjusts orientation incrementally based on the collector's previous position, exhibited noticeable energy losses for larger step sizes. These losses are most pronounced during morning and afternoon periods when the Sun's azimuth changes rapidly. Despite its simplicity and low mechanical demand, the rSAT mechanism tends to accumulate tracking error with coarse angular resolution, leading to a less uniform irradiance profile throughout the day.

A key finding of this study is the nonlinear dependence of thermal energy gain on rotation step size. The quadratic regressions fitted to the simulation results reveal that tracking precision below $\psi = 5°$ brings only marginal benefits, while energy performance declines significantly for $\psi \geq 30°$. This trend indicates the existence of a practical optimum between $\psi = 10°$ and 15°, where mechanical simplicity is preserved without a major sacrifice in energy yield.

From an application perspective, such moderate tracking resolution is well suited for small-scale or building-integrated solar thermal systems, where simplicity, robustness, and low maintenance are crucial design factors. Even with relatively coarse tracking, energy collection efficiency remains high, making the approach attractive for low-energy and near-zero-energy buildings (nZEBs) operating in temperate climates.

It should be emphasized that the present model is intentionally simplified to isolate the influence of geometry and control logic. Effects such as transient thermal behavior, actuator dynamics,

Table 3. Estimated useful thermal energy gain (Q_a) for flat-plate solar collector under absolute (aSAT) and relative (rSAT) tracking strategies, calculated for various rotation step angles (ψ) assuming constant thermal efficiency $\eta_{th} = 0.65$ and absorber area $A = 0.40$ m²

Rotation step ψ [°]	aSAT Q_a [Wh/day]	rSAT Q_a [Wh/day]
1	96.9	95.3
2	96.2	94.6
5	95.7	93.5
10	94.2	90.8
15	92.4	87.8
30	88.8	83.7
45	84.6	80.4
90	81.4	77.7

Table 4. Estimated thermal energy output using temperature-dependent efficiency model

Strategy	ψ [°]	Daily gain [Wh]	Annual gain [kWh]
aSAT	1	88.3	15.89
aSAT	15	84.2	15.15
aSAT	90	74.2	13.35
rSAT	1	86.8	15.63
rSAT	15	80.0	14.40
rSAT	90	73.0	13.35

wind load, and shading were not included in this stage. Nevertheless, the introduction of the temperature-dependent collector efficiency provided a more realistic assessment of thermal performance, reducing estimated daily gains by about 9% compared to constant-efficiency assumptions.

Future research should focus on experimental validation using physical test rigs and on extending the model to seasonal and multi-climatic analyses. Additionally, coupling the geometric tracking algorithm with advanced differential methods—for instance, the Adomian decomposition technique or moving-boundary formulations—could enable more accurate simulation of dynamic heat transfer processes within the absorber plate. These improvements would provide a deeper understanding of transient behavior and further refine predictive capabilities for solar tracking systems.

CONCLUSIONS

This study presented a numerical analysis of Sun-tracking strategies for flat-plate solar collectors, focusing on the effects of rotation step size (ψ) and control strategy on thermal performance. Sixteen configurations were evaluated by combining two tracking modes – aSAT and rSAT—with eight discrete rotation step angles $\psi = \{1°, 2°, 5°, 10°, 15°, 30°, 45°, 90°\}$.

The results demonstrate that both the tracking strategy and the chosen rotation interval have a pronounced influence on the collected solar energy. The aSAT strategy consistently achieved higher energy yields—by up to 17% compared to rSAT—especially at fine rotation steps ($\psi \leq 10°$). However, as ψ increased, both strategies exhibited diminishing returns, confirming the nonlinear relationship between tracking precision and thermal gain.

An optimal range of $\psi = 10–15°$ was identified as a practical compromise between energy performance and mechanical simplicity. Within this range, the collector maintained over 90% of the energy captured by continuous tracking, indicating that moderate angular resolution is sufficient for efficient solar thermal operation.

Future work should focus on experimental validation of the proposed tracking model, including seasonal variations and real-world dynamic effects such as actuator delay, shading, and thermal inertia. The numerical framework developed in this study can also be extended using advanced differential methods, such as the Adomian decomposition approach, to couple transient thermal and radiative processes in solar collector systems.

REFERENCES

1. Tian, Y. and Zhao, C.Y. A review of solar collectors and thermal energy storage in solar thermal applications. Applied Energy, 2013; 104, 538–553. https://doi.org/10.1016/j.apenergy.2012.11.051
2. Rahman, S.A., Varma, R.K. and Vanderheide, T. Generalised model of a photovoltaic panel. IET Renewable Power Generation, 2014; 8(3), 217–229. https://doi.org/10.1049/iet-rpg.2013.0094
3. Riffat, S.B. and Cuce, E. A review on hybrid photovoltaic/thermal collectors and systems. International Journal of Low-Carbon Technologies, 2011; 6(3), 212–241. https://doi.org/10.1093/ijlct/ctr016
4. Garrison, J.D. Optimization of a fixed solar thermal collector. Solar Energy, 1979; 23(2), 93–102. https://doi.org/10.1016/0038-092X(79)90108-7
5. Racharla, S. and Rajan, K. Solar tracking system–a review. International Journal of Sustainable Engineering, 2017; 10(2), 72–81. http://dx.doi.org/10.1080/19397038.2016.1267816
6. Baouche, F.Z., Abderezzak, B., Ladmi, A., Arbaoui, K., Suciu, G., Mihaltan, T.C., Raboaca, M.S., Hudișteanu, S.V., Țurcanu, F.E. Design and simulation of a solar tracking system for PV. Applied Sciences, 2022; 12, 9682. https://doi.org/10.3390/app12199682
7. Gómez-Uceda, F.J., Moreno-Garcia, I.M., Jiménez-Martínez, J.M., López-Luque, R., Fernández-Ahumada, L.M. Analysis of the influence of terrain orientation on the design of PV facilities with single-axis trackers. Applied Sciences, 2020; 10, 8531.
8. Abu-Khadera, M., Badranb, O., Abdallah, S. Evaluating multi-axes sun-tracking system at different modes of operation in Jordan. Renewable and Sustainable Energy Reviews, 2008; 12, 864–873.
9. Kuttybay, N., Mekhilef, S., Koshkarbay, N., Saymbetov, A., Nurgaliyev, M., Dosymbetova, G., Orynbassar, S., Yershov, E., Kapparova, A., Zholamanov, B., Bolatbek, A. Assessment of solar tracking systems: A comprehensive review. Sustainable Energy Technologies and Assessments, 2024; 68, 103879. https://doi.org/10.1016/j.seta.2024.103879
10. Priyam, A. Solar tracking systems–A review. Journal of Mines, Metals and Fuels, 2023; 71(10), 1725–1736. https://doi.org/10.18311/jmmf/2023/35863
11. Nešović, A., Lukić, N., Kowalik, R., Janaszek, A., Taranović, D., Kozłowski, T. Experimental and numerical comparison of glass tube collector with relative single-axis tracking and flat-plate collector without tracking during cloudy-sky days.

Solar Energy, 2025; 291, 113412. https://doi.org/10.1016/j.solener.2025.113412

12. Alici, H., Esenboga, B., Oktem, I., Demirdelen, T., Tumay, M. Chapter 7: Designing and performance analysis of solar tracker system: A case study of Çukurova region. In: Design, Analysis, and Applications of Renewable Energy Systems Advances in Nonlinear Dynamics and Chaos (ANDC), Academic Press, 2021; 165–184.
13. Mousazadeh, H., Keyhani, A., Javadi, A., Mobli, H., Abrinia, K., Sharifi, A. A review of principle and sun-tracking methods for maximizing solar systems output. Renewable and Sustainable Energy Reviews, 2009; 13, 1800–1818.
14. Batayneh, W., Bataineh, A., Soliman, I., Hafees, S.A. Investigation of a single-axis discrete solar tracking system for reduced actuations and maximum energy collection. Automation in Construction, 2019; 98, 102–109.
15. Mohamad, A., Rahman, M.T.A., Phasinam, K., Bin Mohamad, M.S., Saad, M.A.M., Chionh, S.Y.. Analysis of an Arduino based solar tracking system. Journal of Physics: Conference Series, 2021; 2051, 012011.
16. Dawoud, B.M., Lim, S.C. Performance comparison of fixed and single axis tracker photovoltaic system in large scale solar power plants in Malaysia. Indonesian Journal of Electrical Engineering and Computer Science, 2021; 21, 10–17.
17. Hariri, N.G., AlMutawa, M.A., Osman, I.S., Al-Madani, I.K., Almahdi, A.M., Ali, S. Experimental investigation of azimuth- and sensor-based control strategies for a PV solar tracking application. Applied Sciences, 2022; 12(9), 4758. https://doi.org/10.3390/app12094758
18. Krishna K., Upender, P., Buduma, P., Sarkar, M., Simon, S.P., Gundu, V. Solar tracking systems: Advancements, challenges, and future directions: A review. Energy Reports, 2024; 12, 3566–3583. https://doi.org/10.1016/j.egyr.2024.09.038
19. Abadi, I., Soeprijanto, A., Musyafa, A. Design of Single Axis Solar Tracking System at Photovoltaic Panel Using Fuzzy Logic Controller. In: 5th Brunei International Conference on Engineering and Technology (BICET 2014), 2014; 1–6. Bandar Seri Begawan: IEEE.
20. Alshaabani, A. Developing the design of single-axis sun sensor solar tracking system. Energies, 2024; 17(14), 3442.
21. Agee, J.T., Opok, A.O., De Lazzer, M. Solar tracker technologies: market trends and field applications. Advanced Materials Research, 2007; 18–19(June), 339–344.
22. Bentaher, H., Kaich, H., Ayadi, N., Ben Hmouda, M., Maalej, A., Lemmer, U. A simple tracking system to monitor solar PV panels. Energy Conversion and Management, 2014; 78(February), 872–875.
23. Nešović, A., Kowalik, R.. 2025. Single-glazed vacuum tube collector with snal2o3 selective flat absorber plate and gravity single-stage direct water flow: A comprehensive geometric optimization. Applied Sciences, 15, 1838. https://doi.org/10.3390/app15041838
24. Mil'shtein, S., Asthana, D.N. Sun Tracking as Most Efficient Collection of Solar Energy. In: 2024 IEEE 52nd Photovoltaic Specialist Conference (PVSC), Seattle, WA, USA, 2024; 1721–1727. https://doi.org/10.1109/PVSC57443.2024.10749134
25. Neville, R.C. Solar energy collector orientation and tracking mode. Solar Energy, 1978; 20(1), 7–11. https://doi.org/10.1016/0038-092X(78)90134-2
26. Drago, P.A. A simulated comparison of the useful energy gain in a fixed and a fully tracking flat plate collector. In: Proceedings of the Solar Energy International Progress (SEIP 1978), Cairo, Egypt, June 16–22 1978.
27. Tomson, T., Tamm, G. Performance of flat-plate collectors with two-positional active tracking. Estonian Journal of Engineering, 2007; 13(1), (page numbers not provided).
28. Tomson, T. Discrete two-positional tracking of solar collectors. Renewable Energy, 2008; 33(3), 400–405. https://doi.org/10.1016/j.renene.2007.03.017
29. Maia, C.B., Ferreira, A.G., Hanriot, S.M. Evaluation of a tracking flat-plate solar collector in Brazil. Applied Thermal Engineering, 2014; 73(1), 953–962. https://doi.org/10.1016/j.applthermaleng.2014.08.052
30. Garrison, J.D. A program for calculation of solar energy collection by fixed and tracking collectors. Solar Energy, 2002; 73(4), 241–255. https://doi.org/10.1016/S0038-092X(02)00066-X
31. Marion, W.F., Dobos, A.P. Rotation angle for the optimum tracking of one-axis trackers. National Renewable Energy Laboratory (NREL), Technical Report No. NREL/TP-6A20-58891. 2013.
32. Aghamohammadi, A., Foulaadvand, M.E. Efficiency comparison between tracking and optimally fixed flat solar collectors. Scientific Reports, 2023; 13(1), 12712. https://doi.org/10.1038/s41598-023-39892-y
33. Bahrami, A., Okoye, C.O., Pourasl, H.H., Khojastehnezhad, V.M. Techno-economic comparison of fixed and tracking flat plate solar collectors in the northern hemisphere. Journal of Cleaner Production, 2022; 378, 134523. https://doi.org/10.1016/j.jclepro.2022.134523
34. Kambezidis, H.D., Kavadias, K.A., Farahat, A.M. Solar energy received on flat-plate collectors fixed on 2-Axis trackers: effect of ground albedo and clouds. Energies, 2024; 17(15), 3721. https://doi.org/10.3390/en17153721

35. Neagoe, M., Visa, I., Burduhos, B.G., Moldovan, M.D. Thermal load based adaptive tracking for flat plate solar collectors. Energy Procedia, 2014; 48, 1401–1411. https://doi.org/10.1016/j.egypro.2014.02.158
36. Chekerovska, M., Filkoski, R.V. Efficiency of liquid flat-plate solar energy collector with solar tracking system. Thermal Science, 2015; 19(5), 1673–1684. https://doi.org/10.2298/TSCI150427099C
37. Ajunwa, I., Yawas, D.S., Kulla, D.M., Abdullahi, M.B., Ibrahim, I.U., Jnr, M.I. Performance improvement of an indirect solar dryer with single axis manual tracking system and angular simulation of the flat plate collector reflectors. Arid Zone Journal of Engineering, Technology and Environment, 2020; 16(2), 293–308.
38. Radek, N., Konstanty, J., Pietraszek, J., Orman, Ł.J., Szczepaniak, M., Przestacki, D. the effect of laser beam processing on the properties of WC-Co coatings deposited on steel. Materials 2021; 14, 538. https://doi.org/10.3390/ma14030538
39. Orman, Ł.J., Radek, N., Pietraszek, J., Wojtkowiak, J., Szczepaniak, M. Laser treatment of surfaces for pool boiling heat transfer enhancement. Materials 2023; 16, 1365. https://doi.org/10.3390/ma16041365
40. Turkyilmazoglu, M. A reliable convergent Adomian decomposition method for heat transfer through extended surfaces. International Journal of Numerical Methods for Heat & Fluid Flow, 2018; 28(11), 2551–2566, https://doi.org/10.1108/HFF-01-2018-0003
41. Turkyilmazoglu, M. Combustion of a solid fuel material at motion. Energy. 15 July 2020; 203, 117837. https://doi.org/10.1016/j.energy.2020.117837
42. Climate.OneBuilding.Org. Repository of Building Simulation Climate Data. 2025. https://climate.onebuilding.org/